PHYSICAL REVIEW B
CONDENSED MATTER

THIRD SERIES, VOLUME 40, NUMBER 1 1 JULY 1989

Positron-annihilation studies of the electronic structure of NiO

A. L. Wachs, P. E. A. Turchi, R. H. Howell, Y. C. Jean,* and M. J. Fluss
Lawrence Livermore National Laboratory, Livermore, California 94550

J. H. Kaiser and R. N. West
University of Texas at Arlington, Arlington, Texas 76019

K. L. Merkle
Argonne National Laboratory, Argonne, Illinois 60439

A. Revcolevschi
University of Paris, 94105 Orsay, France
(Received 1 February 1989)

We report the first two-dimensional angular correlation of positron-annihilation radiation (ACPAR) studies of the positron-electron momentum distribution for NiO. The data contain two components: a large, isotropic, corelike electron contribution and a remaining valence-electron contribution. We access the covalency structure by modeling the anisotropy with a linear combination of atomic orbitals–molecular orbital method and a localized ion scheme, within the independent-particle model. We obtain the experimental two-dimensional electron-positron k-space momentum density and find no Fermi surface but significant, small residual variations. The importance and implications of these results for ACPAR studies of the new high-T_c perovskites are discussed.

I. INTRODUCTION

The electronic properties of the transition-metal monoxides have long been a subject of experimental and theoretical interest. In particular, MnO, FeO, CoO, and NiO occupy a special place in condensed-matter physics because they are regarded as prototypes for the Mott-Hubbard insulator concept.[1] These materials are antiferromagnetic, electrically insulating, ionic compounds formed in the rocksalt (NaCl) structure. The oxygen p states are fully occupied; the metal s states are empty, and the metal d states are partially occupied. These properties are incompatible with the predictions of standard band theory. In essence, the discrepancy is resolved by the work of Mott, who argues that the correlation energy between the metallic d electrons opens a gap in the conduction band, thus creating a fully occupied lower band and an unoccupied upper band. This prevents metallic conductivity and allows for antiferromagnetic ordering.[2] More recent and detailed models of the electronic structure incorporating refinements to the Mott-Hubbard scheme for these systems have been developed.[3–5] Nevertheless, the precise details of the electronic structure of the transition-metal monoxides remain controversial.[5]

Some of the experimentally measured electronic and magnetic properties of the transition-metal monoxides are similar to those of the new high-T_c superconducting perovskites. Both La_2CuO_4 and $YBa_2Cu_3O_6$, for example, undergo antiferromagnetic spin ordering.[6,7] La_2CuO_4 is an insulator despite band-theoretical predictions of metallic behavior.[8] Photoemission studies of this system suggest significant electron-electron correlation.[9,10] Charge transport measurements suggest hopping conduction between localized states at low temperature, with diffusive transport at high temperature.[11] The transition-metal monoxides and some of the high-T_c perovskites also share the common structural feature of sixfold-oxygen coordinated transition-metal atoms. Many significant details of the electronic structure of both systems can be modeled in terms of localized electronic states associated with these clusters.[1,4,11–15]

The angular correlation of positron-annihilation radiation (ACPAR) technique is useful for probing the electron momentum density of solids.[16] ACPAR has been used most successfully in investigations of the Fermi-surface topologies of metals,[16] ordered compounds, and

disordered alloys.[17] One-dimensional ACPAR studies have been performed on metal oxides such as NiO (Ref. 18) and Fe_3O_4 (Ref. 19). More recently, ACPAR measurements have been performed on the incomplete perovskite $Na_{0.64}WO_3$,[20] $YBa_2Cu_3O_7$,[21–23] and La_2CuO_4.[12,15,24] The results for La_2CuO_4 and $Na_{0.64}WO_3$ were interpreted in terms of a covalency structure, using a linear combination of atomic orbitals–molecular orbital (LCAO-MO) scheme within the independent-particle model (IPM).[18]

Here we report the first 2D ACPAR measurements of single-crystal NiO for two different crystalline orientations. The anisotropic component of the data is successfully compared with theoretical results based upon a localized-cluster LCAO-MO model within the IPM, first developed by Chiba and Tsuda[18] and later used by others.[12,15,20] Theory and experiment are in qualitative agreement, demonstrating the utility of the cluster model for revealing details of the covalency structure. We discuss the origins of the discrepancies between the calculated and experimental anisotropies. We examine the contributions of all of the NiO positronic and electronic states to the integrated, two-dimensional electron-positron momentum density of states $\rho^{2\gamma}(\mathbf{k})$ by employing the Lock-Crisp-West construction.[25] NiO is a well-known insulator and as expected, we find no evidence for a Fermi surface in $\rho^{2\gamma}(\mathbf{k})$ within the statistical noise limits of our experiment. But there are significant residual variations attributable to positron wave function and electron-positron correlation effects. Finally, we relate our findings to the question of the interpretation of ACPAR electronic structure measurements for the high-T_c perovskites.

II. DESCRIPTION OF EXPERIMENT

The single-crystal NiO sample used in the ACPAR measurements was grown from high-purity NiO powder (99.9995% NiO) at the Argonne National Laboratory using the Verneuil technique in an arc-image furnace. The cylindrically shaped boule so obtained was annealed at 1300 °C in a carbon dioxide and monoxide mixture with $P_{CO_2}/P_{CO}=85$ for 46 h, slowly cooled over a period of several hours to 1100 °C, held for two hours at 1100 °C, and quenched to room temperature in an argon atmosphere. From the defect model of Peterson and Wiley,[26] we estimate the deviation in stoichiometry δ in $Ni_{1-\delta}O$ obtained in this manner to be about 2×10^{-6}.

An experimental specimen was prepared from the NiO boule by sectioning two pieces of identical size with identically oriented faces. The crystalline orientations were determined to within $\pm1°$ by standard Laue x-ray back reflection. After sectioning, the cut faces were lightly polished with a fine silica slurry to remove near-surface damage caused by the sectioning procedure. The two crystals were oriented in approximate ($\pm1°$) registry along their common cubic crystalline axes and "sandwiched" about a ~2 mCi, 1-mm-diam dried deposition of $^{22}NaOC_2H_5$ on ~1 μm of polycrystalline Ni foil (~1.1 mg/cm^2). The sample-source package was subsequently sealed in an Al cell under an ultrahigh-purity ^{4}He atmosphere. The package was cooled to 13 K during the course of the ACPAR measurements to reduce the effects of thermal broadening upon the electron-positron momentum distribution. The positron-annihilation lifetime was measured initially to assess the degree of positron trapping; detectable trapping might complicate the interpretation of the ACPAR data in terms of an extended, Bloch-state positron wave function. Approximately 10^6 counts were accumulated for the NiO crystals at room temperature. We obtained only two lifetime components. The longer one, of magnitude 0.34 ns and intensity 8%, is attributed to surface and source annihilation of Ps and positrons. No more than one remaining lifetime could be resolved from the data. We therefore conclude that only a single bulk lifetime, 137 ± 1 ps, exists in our NiO specimens.

We made other measurements of the bulk positron lifetime for differently prepared NiO samples. For example, the unpolished surfaces of the ACPAR specimen had the same bulk lifetime of 137 ± 1 ps. We performed lifetime measurements on two sections of another boule grown at Argonne National Laboratory using Verneuil methods, and sectioned before annealing but not polished. We obtained a single bulk lifetime of 134 ± 1 ps, and a source component of 0.34 ns and intensity 5%. Another sample grown by float-zone refining techniques from high-purity NiO at the University of Paris-Sud showed a similar bulk lifetime. For these high-purity, nearly defect-free samples, therefore, the positronic Bloch state appears nearly insensitive to small differences in preparation which might affect the concentration of vacancy trapping sites. We believe our lifetime results are representative for high-purity, nearly defect-free single-crystal NiO, and that vacancy trapping is negligible.

We estimate the angular resolution of our ACPAR apparatus (including the effects of positron wave-function thermal broadening) to be ~0.5 mrad. 1 mrad of angular deviation corresponds to a combined electron-positron momentum of $10^{-3}mc$ in the laboratory reference frame, where m is the electron rest mass and c is the speed of light. The sample-source to detector distance was ~9.6 m. Additional details about the ACPAR apparatus will be given elsewhere.[15] We performed the ACPAR measurements in two experimental geometries: with the integration axes parallel to the NiO $\langle100\rangle$ and $\langle110\rangle$ axes. Approximately 41×10^6 counts were collected for each geometry using a square 256×256 matrix with a bin width of 0.208 mrad ($\sim10^4$ counts peak channel).

III. RESULTS AND DISCUSSION

Figure 1 shows an isodensity plot and radial section of the electron-positron momentum distribution obtained by ACPAR with integration along the $\langle100\rangle$ axis of NiO. The distribution is highly isotropic, a characteristic result for ACPAR measurements of oxometallates.[12,15,18,20–24] A similar result is seen for the ACPAR distribution for NiO integrated along the $\langle110\rangle$ direction (not shown). To interpret these findings, we recall[27] that the ACPAR technique measures the "real-space" electronic momen-

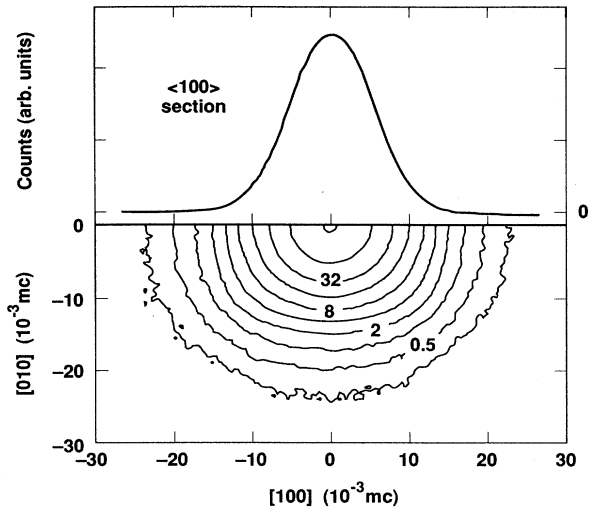

FIG. 1. Experimental 2D ACPAR electron-positron momentum distribution for NiO: integration direction ⟨100⟩. The top inset displays a radial section through the distribution along the ⟨100⟩ axis. The bottom inset is an isodensity contour plot. The percentage values of the distribution maximum are labeled for selected isodensities.

tum density $\rho^{2\gamma}(\mathbf{p})$ of electrons in a crystal (as modulated by the positron momentum distribution) and not the electronic crystal-momentum distribution in k space.

Thus, for example, in a metal one can interpret 2D angular correlation distributions as arising from (i) states in full Brillouin zones which contribute a continuous distribution having the point symmetry of the reciprocal lattice, and (ii) contributions from partially filled zones which are nonvanishing only at a momentum $\mathbf{p}$ such that $\mathbf{p}-\mathbf{G}$ lies inside the Fermi surface.[25] In an insulator the contributions (ii) are absent.

NiO is a well-known insulator. Consistent with this experimental fact, we find no evidence of a Fermi surface in $\rho^{2\gamma}(\mathbf{p})$. For example, upon closer examination there are no observable "Fermi breaks" due to partially filled band contributions[16] in the data of Fig. 1. The highly isotropic nature of the ACPAR distribution suggests a significant "core" contribution.[12,18–20] In the next portion of the discussion, we shall assume that this is the case and restrict ourselves to a model description of the evidently small anisotropic, valence-electron component of the NiO 2D ACPAR distributions. In our treatment, we examine the contribution of selected, antibonding valence states to the anisotropy, and ignore the "core" contribution to the same. Our approach is approximate, qualitative, and lacks rigor. Nevertheless, it provides a preliminary description of the covalency structure in a correlated-electron solid in the absence of more sophisticated electronic structure calculations.

A. Analysis of the ACPAR distribution anisotropies

The work of Chiba,[18,19] Akahane *et al.*,[20] Wachs *et al.*,[12] and Turchi *et al.*[15] provides an appealing and intuitive way for modeling the valence states in NiO. Therein it is shown that an electronic wave function of given symmetry (for instance a p state) transforms into a function of the same point-group symmetry in momentum space. Thus one can obtain access to the covalency structure by a point-group symmetry decomposition of the electronic wave-function contributions to $\rho^{2\gamma}(\mathbf{p})$. Following Refs. 12, 15, 18, and 19, we choose for our electronic wave functions a basis set derived using the LCAO-MO formalism in conjunction with a localized ion scheme within the IPM. We ignore the translational symmetry of the lattice and adopt a ligand-field theory approach by modeling a representative Ni-O octahedron. Some effects of these assumptions upon the calculated $\rho^{2\gamma}(\mathbf{p})$ will be discussed below.

Detailed descriptions of our LCAO-MO formalism and its derivation have been given elsewhere.[15,18,19] We therefore restrict ourselves to describing the details specific to our NiO system. For the sake of simplicity, we assume that the nickel atom is only surrounded by six oxygen atoms, in an octahedral configuration. We form antibonding combinations of the $3d$ nickel orbitals with the $2s$ and $2p$ oxygen orbitals.[28] In this model, the atomic wave functions of Ni^{2+} are in a d^8 configuration and are obtained from a Herman-Skillman scheme,[29] and the atomic wave functions $2s$ and $2p$ of O^{2-} (in a $1+$ well) are given by Watson.[30] Nickel oxide has a rhombohedral structure below 210±4 °C. However, the trigonal distortion from the NaCl structure is small (of order 0.1%).[31] We neglect the distortion and assume a cubic, face-centered lattice with $a=4.177$ Å.

Ignoring the antiferromagnetic ordering of the NiO lattice,[32] the five $3d$ levels of Ni will then be split by a cubic crystal field into a triply degenerate t_{2g} below a doubly degenerate e_g level.[33,34] The t_{2g} type of molecular symmetry orbitals involves mixing between the Ni $3d_{xy}$, $3d_{yz}$, and $3d_{xz}$ and the O $2p_x$ and O $2p_y$, the O $2p_y$ and O $2p_z$, and the O $2p_x$ and O $2p_z$ orbitals, respectively. The e_g type of symmetry molecular orbitals involve mixing between the Ni $3d_{z^2}$, O $2p_z$, and O $2s$, and the Ni $3d_{x^2-y^2}$ and O $2p_y$, and O $2s$ orbitals.

The positronic wave function, in a Bloch state with zero momentum, is approximated by a variational function using a procedure due to Chiba[15,18,19] which takes properly into account the fairly localized electronic character of the material and also the relative affinity of the positron to the different chemical species. We model the NiO charge density as a superposition of neutral Herman-Skillman atomic charge distributions.[29] This assumption is qualitatively valid. For example, theoretical investigations of extended x-ray-absorption fine-structure (EXAFS) and x-ray-absorption near-edge structure (XANES) electron-scattering phase shifts in ionic materials (CaO) have shown that the scattering potentials can be effectively modeled by using neutral, atomic charge distributions.[35] Our scheme also compares favorably to other positronic calculations for related oxometallates (high-T_c perovskites) in the same regions of interest.[12,13,15,22] We display isodensity contour plots of the positron densities in two planes representative of the crystal NiO in Fig. 2.

We extracted the anisotropic features from the under-

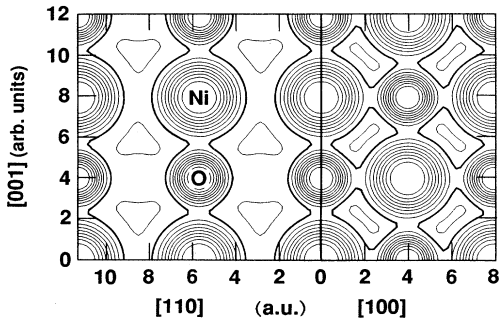

FIG. 2. Planar isodensity contour plot of the square of the positron wave function for NiO, calculated by the method of Ref. 18. The right-hand side shows isodensity information in the {100} Ni-O atomic plane; to its left, and joined along a common boundary, is the corresponding information for the {110} Ni-O plane. The principal atomic sites of Ni and O have been labeled. Highlighted levels enclose the regions (between the atoms and in the interstices) of highest positron probability ($\geq 90\%$ of the maximum probability).

lying, isotropic experimental distribution by subtracting annular radial-averaged reference values form the two-dimensional distributions for each of the two experimental geometries. The resulting experimental "residual" spectra for the ⟨100⟩ and ⟨110⟩ integration geometries are shown in Figs. 3(a) and 3(b), respectively. In Figs. 4(a) and 4(b) we display the residual anisotropies obtained from LCAO-MO calculations for each of the two respective geometries. The calculated electron-positron momentum distribution is simply given by the overlap of the positronic wave function with the electronic LCAO-MO wave functions.[18,19]

The three covalency-overlap parameters so introduced were qualitatively fitted to the data by comparison of the theoretical and experimental anisotropies. We found the calculated anisotropies to be sensitive to the degree of σ and π bonding, but relatively insensitive to the degree of s bonding. The amounts of σ and π bonding introduced significantly affected the relative amplitudes of the theoretical anisotropy features but left their locations unchanged. We chose the combination of the three covalency parameters which gave the best agreement between theory and experiment (see below). The covalency parameters have the following values:

$$c_\sigma = 0.3400; \quad c_\pi = 0.0180; \quad c_s = 0.0700 .$$

Here the standard subscript notations σ and π, and s refer to the appropriate bond symmetries involving overlaps between the Ni $3d$ and O $2p$, and Ni $3d$ and O $2s$ orbitals, respectively.

A larger covalency-overlap parameter indicates greater mixing between the orbitals in question. As expected, we find from the relative magnitudes of the covalency-overlap parameters that the t_{2g} orbitals are principally of Ni $3d$ character, and the Ni-O interatomic bonding is primarily of e_g character and σ symmetry. The O $2s$ contri-

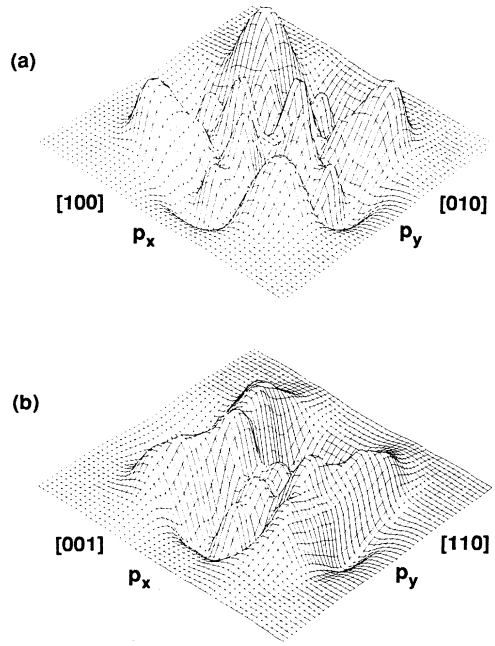

FIG. 3. Experimental residual anisotropy surfaces (see text) of two-dimensional positron-electron momentum distributions for NiO with integration directions perpendicular to the indicated cubic crystalline axes. Points outside the outermost complete annuli have been set to zero. The values of p_x and p_y are in the range $\pm 26.1 \times 10^{-3} mc$.

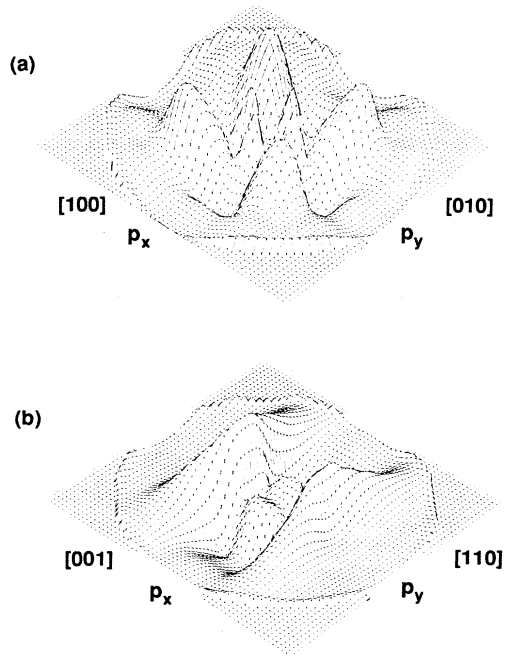

FIG. 4. Theoretical residual anisotropy surfaces (see text) of two-dimensional positron-electron momentum distributions for NiO with integration directions perpendicular to the indicated cubic crystalline axes. Points outside the outermost complete annuli have been set to zero. The values of p_x and p_y have the same range as indicated for Fig. 3.

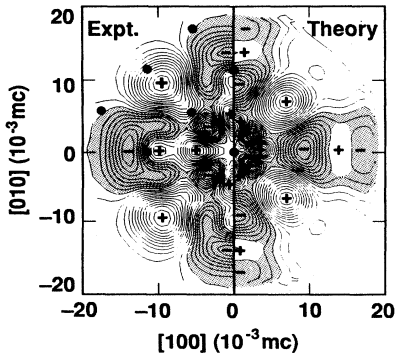

FIG. 5. Experimental (theoretical) isodensity contour plots of the residual anisotropy surfaces for the NiO ⟨100⟩ integration axis [see Figs. 3(a) and 4(a)] are displayed in the left (right) insets. Negative values have been highlighted. The small, solid circles in the experimental inset show the (p_x,p_y) coordinates of $\Gamma X\Gamma$ points projected upon the detector plane.

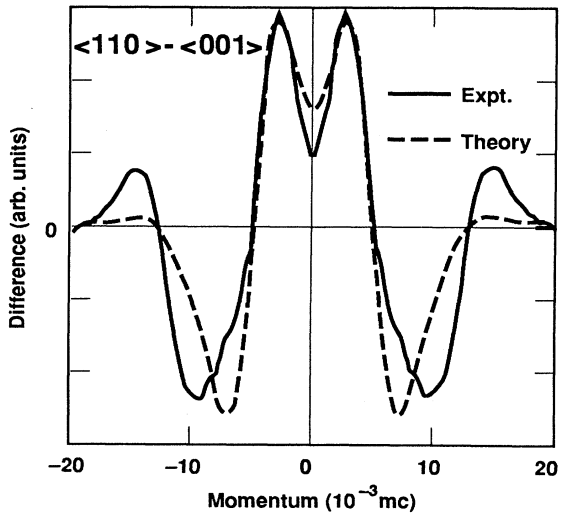

FIG. 7. Experimental (theoretical) difference curves formed by taking the difference between projections of the two-dimensional experimental (theoretical) positron-electron annihilation momentum distributions for NiO along the indicated pair of cubic crystalline axes. The experimental (theoretical) curves are denoted by solid (dashed) lines.

bution is small. A similar, qualitative description holds for details of the Cu-O cluster interatomic bonding and covalency structure for La_2CuO_4 obtained from ACPAR measurements.[12,15]

We display isodensity contour plots of the anisotropies for additional comparison of theory and experiment in Fig. 5 (Fig. 6) for the ⟨100⟩ (⟨110⟩) integration geometry. Experiment (theory) are shown in the left (right) insets of each plot. Negative values have been highlighted. The dots in the upper halves of the experimental insets show the positrons of the projected Γ points. Qualitatively, theory and experiment compare favorably in terms of overall symmetry and relative peak extrema. The two-peak structure which occurs at low momenta in Figs. 3(b), 4(b), and is associated with the e_g type of symmetry molecular orbital. The broad, four-peak structure at higher momenta in Figs. 3(a), 4(a), and 5 is associated with the t_{2g} type of molecular symmetry orbital.

Figure 7 shows the curve (solid line) obtained from the full experimental 2D ACPAR distribution for NiO in the ⟨110⟩ integration geometry by taking the difference between projections of the distribution along the ⟨110⟩ and ⟨100⟩ crystalline axes. The corresponding anisotropic difference curve from our LCAO-MO calculations is displayed using a dashed line; theory and experiment are in reasonable, qualitative agreement. The differences are expressed in terms of arbitrary units. In the experimental curve, they correspond to an anisotropy no greater than ~0.6% of the counts in any channel of the ⟨110⟩ or ⟨100⟩ distribution projections.

One can make a crude estimate of the percentage of the experimental ACPAR electron-positron momentum distributions modeled by the theoretical, LCAO-MO calculations. Normalization of the extremal theoretical and experimental anisotropic residual variations (represented by peak-to-valley amplitudes), or the sums of residuals in both types of anisotropy surfaces, indicates that the total theoretical valence contribution to the experimental distributions is between 10% and 20%. There is a significant margin of error and uncertainty because of the quantitative discrepancies between the theoretical and experimental anisotropies.

A more detailed comparison of theory and experiment shows significant discrepancies in peak location and additional experimental residual surface features not present in the calculated LCAO-MO. The discrepancies which occur at high momentum may be partly attributed to electronic transfer between nearest-neighbor nickel atoms, and a more rapid decrease in the radial component of the momentum wave functions than anticipated in our model. We have also neglected the consequence of the well-known antiferromagnetic ordering of Ni spins in NiO (Ref. 32) upon the crystal-field splitting. In the

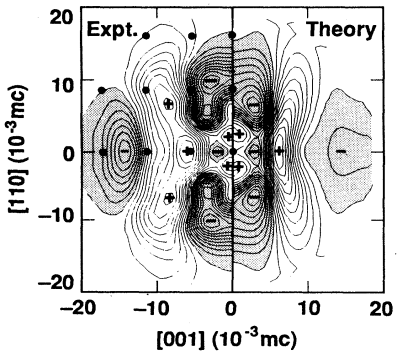

FIG. 6. Same as Fig. 5, but for the NiO ⟨110⟩ integration axis [see Figs. 3(b) and 4(b)]. The small, solid circles in the experimental inset show the (p_x,p_y) coordinates of $\Gamma K\Gamma$ points projected upon the detector plane.

antiferromagnetic lattice the orbitals belonging to e_g and t_{2g} are not the basis functions of the irreducible representations of the crystalline point-symmetry group; thus our occupancy scheme is not strictly correct.[3] Other discrepancies may arise from our derivation of the positronic wave function from a localized-ion lattice model. And we have not modeled the "core" contribution to the anisotropy above.

B. The *k*-space electron-positron momentum densities

We have shown that crystal-field theory can give a satisfactory, qualitative description of the anisotropic component of NiO and other oxometallate 2D ACPAR distributions.[12,15] Our analysis was restricted to a small subset of the electronic states, namely antibonding combinations of $3d$ metallic orbitals with oxygen $2s$ and $2p$ orbitals. We now examine the contribution of all NiO electronic and positronic states to the electron-positron **k**-space momentum density (EMD) $\rho^{2\gamma}(\mathbf{k})$. The results are compared to the constant EMD expected for an insulating, IPM system in which the perturbation of the probing positron is negligible.

There is a direct relationship between the electron-positron momentum density $\rho^{2\gamma}(\mathbf{p})$ measured in an ACPAR experiment and the occupancy of electronic states in **k** space, or EMD. Lock *et al.*,[25] Lock and West,[36] and Beardsley *et al.*[37] have developed a superposition procedure (hereafter referred to as "LCW") whereby the experimentally measured electron-positron momentum density $\rho^{2\gamma}(\mathbf{p})$ is transformed into the Bloch wave vector EMD $\rho^{2\gamma}(\mathbf{k})$. In this distribution, the singularities and other features that reflect a Fermi surface are isolated and emphasized; the perturbations caused by positron wave-function and electronic correlation effects often appear as a smaller [relative to their effect on $\rho^{2\gamma}(\mathbf{p})$] perturbation of $\rho^{2\gamma}(\mathbf{k})$ from the equivalent, purely electronic **k**-space density $\rho_e(\mathbf{k})$. The results are directly interpretable in terms of $\rho_e(\mathbf{k})$ if the positron samples all valence electronic states equally and the IPM is valid.[25,36] The power of this technique to establish the essential topology of a complex Fermi surface of several sheets in metals, through simple and easily readable contour displays, has now been established in several works.[38,39] However, it is more difficult to interpret the results of LCW in terms of a Fermi surface when the residual EMD variations are small and electron-electron correlation, "core" contributions, and positronic wave-function effects may be significant. This is the case for oxometallate systems.[15,40]

We have applied the LCW formalism to our NiO data. Figure 8 shows an isodensity contour plot of the two-dimensional $\rho^{2\gamma}(\mathbf{k})$ for the two experimental integration axes ⟨100⟩ and ⟨110⟩. Projected Brillouin-zone boundaries and symmetry points have been labeled. To derive the approximate EMD, we used the Brillouin zone for the fcc lattice, with $\mathbf{G}=(2\pi/\mathbf{a})\langle 111\rangle$ and $a=4.177$ Å. The minimum value is about 98% of the maximum, a result close to filled-band behavior.[15,25,37,40] There are on the average of $\sim 6\times 10^4$ counts per channel in each EMD, giving a corresponding statistical noise limit of the order of 0.1%. We therefore believe that the residual variations of Fig. 8 are significant and require further explanation.

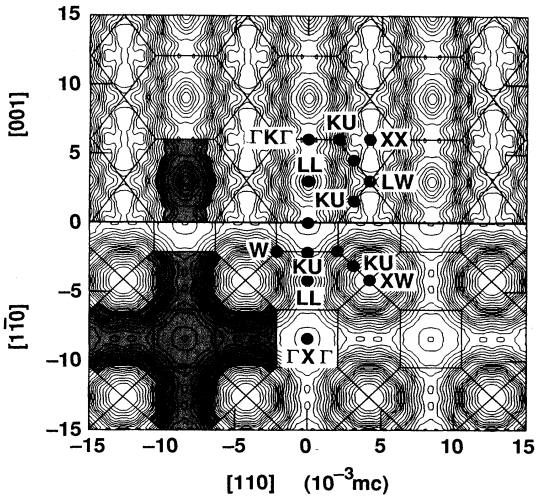

FIG. 8. Extended-zone isodensity contour plots of the two-dimensional positron-electron *k*-space momentum densities for the NiO ⟨100⟩ and ⟨110⟩ integration geometries obtained by the Lock-Crisp-West superposition procedure of Ref. 25. The integration axis for the top (bottom) inset is ⟨110⟩ (⟨100⟩). Major symmetry points have been labeled and the boundaries of the projected Brillouin zones are displayed for each inset. The maximum-to-minimum variation is ~2% or ~3%, and residual values below the median residual value have been highlighted in representative Brillouin zones.

Because there is no independent experimental evidence in favor of a Fermi surface in NiO, we must look elsewhere to explain the residual variations in the EMD. Positron wave-function effects are likely responsible for the residual variations in the NiO 2D EMD results. Similar, small residual variations have been observed for derived 2D EMD from 2D ACPAR measurements for La_2CuO_4,[15,40] and for 1D EMD for the semiconductor (narrow band-gap insulator) Ge.[37] In oxometallates (unlike metals), the interatomic bonding has covalent character and the positron is anisotropically excluded from a significant portion of the crystalline free volume. The oxometallate systems also offer a lattice of inequivalent sites to the sampling, Bloch-state positron. Thus there are significant variations of the electron-positron overlap in the regions between the atoms and in the interstices (see Fig. 2 and Ref. 41). It is possible that the positronic ground state may not be purely *s* wave in character, and the data of Fig. 8 may be influenced by small but significant positron-electron overlap modulations, such as preferential annihilation between states of certain electronic and positronic angular momenta.[39] More detailed calculations of the positronic wave functions in oxometallates, semiconductors, etc. and their contribution to the EMD are required to clarify this point.

Electron-electron correlation effects may also contribute a superstructure to the EMD by creating a broad, experimentally unresolved gap over the Brillouin zone. Despite its nominal resemblance to the EMD Fermi-

surface "signature" of a metal,[16] the origin of this superstructure lies in the symmetry of the NiO antiferromagnetic spin lattice, not the contribution of partially filled bands.[42] Electronic structure calculations, perhaps involving states of a localized character, are necessary to quantify this effect.

IV. SUMMARY AND CONCLUSIONS

It has been shown in this work and elsewhere[12,15,20,40] that positron-annihilation spectroscopy is a potentially valuable technique for probing the electronic structure of oxometallates. Experimentally, the NiO ACPAR distributions are highly isotropic, with a small anisotropic component. The 2D ACPAR residual anisotropy surfaces and those derived from a LCAO-MO scheme compare favorably. The qualitative agreement between the cluster-model theory and experiment suggests the positron is very sensitive to details of the metal-ligand bonding. We obtain access to the covalency structure of NiO. Significant, quantitative discrepancies between theory and experiment illustrate the need for more sophisticated electronic and positronic band-structure calculations to model $\rho^{2\gamma}(\mathbf{p})$ and its anisotropic component. The insulating properties of NiO are reflected in the absence of a Fermi surface in its 2D EMD and the absence of partially filled band discontinuities in the full 2D ACPAR distributions. The small residual variations (~ 2–3%) in the EMD are likely due to positronic wave-function effects, though the contributions of electron-electron correlation cannot be ruled out. Similar conclusions have been reached for La_2CuO_4.[12,15,40]

The overall structure of the anisotropies of the experimental and theoretical momentum distributions are in good qualitative agreement and are consistent with the prominence of the hybridization of the Ni $3d$ and O $2s$ orbitals. That the two anisotropies differ as to the relative location of maxima and minima is not surprising, since the theoretical calculations are based upon a simplistic LCAO-MO model which neglects the Bloch periodicity. What is surprising is that the peaks in the experimental anisotropies do not coincide with all of the points of the projected reciprocal lattice (see Figs. 5 and 6), as would be expected from our naive understanding of the momentum distribution for single-atom basis crystals. In most cases we observe that the approximate zeroes of the experimental anisotropies coincide with these points. The explanation for this behavior may well lie in the IPM prescription for the electron-positron momentum distribution for the NaCl structure:

$$\rho^{2\gamma}(\mathbf{p})=2\Omega\sum_j \Theta(E_F-E_{\mathbf{k},j})\sum_G \delta(\mathbf{p}-\mathbf{k}-\mathbf{G})[\,|C^a_{\mathbf{G},j}(\mathbf{k})|^2+|C^b_{\mathbf{G},j}(\mathbf{k})|^2+e^{-i\mathbf{G}\cdot\mathbf{d}}C^a_{\mathbf{G},j}(\mathbf{k})C^{*b}_{\mathbf{G},j}(\mathbf{k}) +e^{+i\mathbf{G}\cdot\mathbf{d}}C^{*a}_{\mathbf{G},j}C^b_{\mathbf{G},j}(\mathbf{k})]\ ,$$

where

$$C^\alpha_{\mathbf{G},j}(\mathbf{k})=\Omega^{-1}{}_{\Omega^\alpha}\int d^3r e^{-i(\mathbf{k}+\mathbf{G})\cdot\mathbf{r}}\phi^\alpha_{\mathbf{k},j}(\mathbf{r})\phi^\alpha_+(\mathbf{r})\ .$$

Here Ω is the volume of the Wigner-Seitz cell, the superscript α distinguishes quantities associated with the two different atoms a and b of the basis, $\mathbf{G}$ is a reciprocal-lattice vector (of the fcc lattice), and $\mathbf{d}=(a/2)(1,1,1)$ is the basis vector between the Ni and O atoms. $\Theta(x)$ is the Heaviside unit step function (the Fermi-Dirac distribution at zero temperature), E_F is the electron Fermi energy, and $E_{\mathbf{k},j}$ and $\phi^\alpha_{\mathbf{k},j}(\mathbf{r})$ are, respectively, the energy and wave function of the electron state of wave vector $\mathbf{k}$ and band index j. $\phi_+(\mathbf{r})$ is the positron wave function.

The reciprocal-lattice vectors for the NaCl structure fall into two categories: "odd" and "even" as defined by the sum of their indices. For odd reciprocal-lattice points [e.g., (111)] the phase factor $e^{\pm i\mathbf{G}\cdot\mathbf{d}}$ in the expression for $\rho^{2\gamma}(\mathbf{p})$ takes on the value -1. Positive interference terms $C^\alpha_{\mathbf{G},j}(\mathbf{k})C^{*\alpha'}_{\mathbf{G},j}(\mathbf{k})$ would then explain the diminution of $\rho^{2\gamma}(\mathbf{p})$ at these odd values of $\mathbf{G}$. However, for the even reciprocal-lattice points [e.g., (200)], $e^{\pm i\mathbf{G}\cdot\mathbf{d}}=+1$, so that negative cross terms would be required to explain the positional discrepancies of the extrema in the experimental anisotropies. To ascertain whether the quantitative discrepancies are due to such simple effects would only require extraction of the cross terms during the improved calculations mentioned above.

We believe the qualitative similarity between the findings for these transition-metal oxides and perovskites suggests common features in their electronic structure. The Bloch-state positron has the capability to probe these features at the level of the metal-oxygen interatomic bonding and access the covalency structure.[12,13,15] The positronic sensitivity to these particular details of the electronic structure may be due to significant positron-electron overlap differences between states of certain electronic and positronic angular momenta. The NiO Bloch-state positronic wave function may not be the trivial, purely s-wave ground state assumed in the analysis of ACPAR results from metals.[13,15,16,22,25,40] By analogy with NiO, therefore, one must use great care in the interpretations of 2D EMD results obtained by the LCW construction for the correlated-electron, insulating perovskite materials.[25,40] Recent comparisons of the experimental and calculated $\rho^{2\gamma}(\mathbf{p})$ for $YBa_2Cu_3O_7$ illustrate the necessity for detailed positronic wave-function calculations for these systems.[43]

The metallic, superconducting, high-T_c perovskites $La_xSr_{1-x}CuO_{4-\delta}$ and $YBa_2Cu_3O_{7-\delta}$ are derivable from their nonsuperconducting, antiferromagnetic insulator "parents" by impurity doping or oxygenation. The effect of these modifications upon the "parent" electronic structure are not well understood, particularly upon the features of the EMD as derived from ACPAR measurements.[12,24,42] We are addressing this problem and the

problems of "parent" EMD interpretation by investigating the metal-to-insulator phase transition in these systems with ACPAR. In view of the possibility that the positronic perturbations upon $\rho^{2\gamma}(\mathbf{p})$ and the EMD are significant,[43] it would also be worthwhile to measure $\rho_e(\mathbf{p})$ and $\rho_e(\mathbf{k})$ *without* the positron for transition-metal oxides and high-T_c perovskites. Such experiments are now feasible because newly developed Compton-scattering techniques have a resolution comparable with ACPAR.[44] Finally, there is a need to develop more sophisticated theoretical treatments involving electronic states of a localized character to model the electronic structure of these complicated, incompletely understood systems.

ACKNOWLEDGMENTS

This work was performed under the auspices of the U.S. Department of Energy by the Lawrence Livermore National Laboratory under Contract No. W-7405-ENG-48. Work at the Argonne National Laboratory (ANL) was supported by the U.S. Department of Energy Office of Basic Energy Sciences–Materials Science under Contract No. W-31-109-ENG-38. We are grateful for the assistance of J. F. Reddy and C. L. Wiley at ANL. One of us (J.H.K.) would also like to thank the Robert A. Welch Foundation (Grant No. Y-1135) for partial support for this work. We wish to acknowledge valuable discussions with P. A. Sterne.

---

*Permanent address: University of Missouri–Kansas City, Kansas City, MO 64110.

[1]N. F. Mott, Proc. Phys. Soc. London, Sect. A **62**, 416 (1949); D. Adler and J. Feinleib, Phys. Rev. B **2**, 3112 (1970); B. H. Brandow, Int. J. Quantum Chem., Symp. **10**, 417 (1976); Adv. Phys. **26**, 651 (1977); B. Koiler and L. M. Falicov, J. Phys. C **7**, 299 (1974); **8**, 695 (1975); A. B. Kunz and G. T. Surratt, Solid State Commun. **25**, 2989 (1978); A. B. Kunz, Int. J. Quantum Chem., Symp. **15**, 487 (1981).

[2]N. F. Mott, *Metal-Insulator Transitions* (Taylor and Francis, London, 1974).

[3]K. Terakura, A. R. Williams, T. Oguchi, and J. Kubler, Phys. Rev. Lett. **52**, 1830 (1984).

[4]G. A. Sawatzky and J. W. Allen, Phys. Rev. Lett. **53**, 2339 (1984).

[5]J. Zaanen, G. A. Sawatzky, and J. W. Allen, Phys. Rev. Lett. **55**, 418 (1985).

[6]D. Vaknin *et al.*, Phys. Rev. Lett. **58**, 2802 (1987); S. Mitsuda *et al.*, Phys. Rev. B **36**, 822 (1987); T. Freltoft *et al.*, *ibid.* **36**, 826 (1987); Y. J. Uemura *et al.*, Phys. Rev. Lett. **59**, 1045 (1987); G. Shirane *et al.*, *ibid.* **59**, 1613 (1987); Y. Endoh *et al.*, Phys. Rev. B **37**, 7443 (1988).

[7]M. Sato, S. Shamoto, J. M. Tranquada, G. Shirane, and B. Keimer, Phys. Rev. Lett. **61**, 1317 (1988); J. M. Tranquada *et al.*, *ibid.* **60**, 156 (1988); J. M. Tranquada *et al.*, Phys. Rev. B **38**, 2477 (1988).

[8]See, for example, L. F. Mattheis, Phys. Rev. Lett. **58**, 1028 (1988).

[9]See, for example, A. Fujimori, E. Takayama-Muromachi, Y. Uchida, and B. Okai, Phys. Rev. B **35**, 8814 (1987); J. A. Yarmoff, D. R. Clarke, W. Drube, U. O. Karlsson, A. Taleb-Ibrahimi, and F. J. Himpsel, *ibid.* **36**, 3967 (1987).

[10]H. Eskes and G. Sawatzky, Phys. Rev. Lett. **61**, 1415 (1988).

[11]S.-W. Cheong, Z. Fisk, R. S. Kwok, J. P. Remeika, J. D. Thompson, and G. Gruner, Phys. Rev. B **37**, 5916 (1988).

[12]A. L. Wachs, P. E. A. Turchi, Y. C. Jean, K. H. Wetzler, R. H. Howell, M. J. Fluss, D. R. Harshman, J. P. Remeika, A. S. Cooper, and R. M. Fleming, Phys. Rev. B **38**, 913 (1988).

[13]Y. C. Jean, J. Kyle, H. Nakanishi, P. E. A. Turchi, R. H. Howell, A. L. Wachs, M. J. Fluss, R. L. Meng, H. P. Hor, J. Z. Huang, and C. W. Chu, Phys. Rev. Lett. **60**, 1069 (1988).

[14]A. Fujimori and F. Minami, Phys. Rev. B **30**, 957 (1984), and references therein.

[15]P. E. A. Turchi, A. L. Wachs, Y. C. Jean, R. H. Howell, K. H. Wetzler, and M. J. Fluss, Physica B+C **153-155C**, 157 (1988); P. E. A. Turchi *et al.* (unpublished).

[16]See, for example, S. Berko, in *Positron Solid State Physics*, edited by W. Brandt and A. Dupasquier (North-Holland, Amsterdam, 1983).

[17]P. E. Mijnarends, Phys. Status Solidi A **102**, 31 (1987).

[18]T. Chiba and N. Tsuda, Appl. Phys. **5**, 37 (1974).

[19]T. Chiba, J. Chem. Phys. **64**, 1182 (1976).

[20]T. Akahane, K. R. Hoffman, T. Chiba, and S. Berko, Solid State Commun. **54**, 823 (1985).

[21]A. A. Manuel, Helv. Phys. Acta **61**, 451 (1988); L. Hoffman, A. A. Manuel, M. Peter, E. Walker, and M. A. Damento, Europhys. Lett. **6**, 61 (1988); Physica B+C **153-155C**, 129 (1988).

[22]E. C. von Stetten, S. Berko, X. S. Li, R. R. Lee, J. Byrnestad, D. Singh, H. Krakauer, W. E. Pickett, and R. E. Cohen, Phys. Rev. Lett. **60**, 2198 (1988).

[23]L. C. Smedskjaer, J. Z. Liu, R. Benedek, D. G. Legnini, D. J. Lam, M. D. Stahulak, and A. Bansil, Physica B+C **156C**, 269 (1988).

[24]S. Tanigawa, Y. Mizuhara, Y. Hidaka, M. Oda, M. Suzuki, and T. Murakami, in Proceedings of the Eighth International Conference on Positron Annihilation, Gent, Belgium, 1988, (World Scientific, Singapore, 1988).

[25]D. G. Lock, V. H. C. Crisp, and R. N. West, J. Phys. F **3**, 561 (1973).

[26]N. L. Peterson and C. L. Wiley, J. Phys. Chem. Solids **46**, 43 (1985).

[27]R. N. West, Adv. Phys. **22**, 263 (1973).

[28]J. O. Owen and J. H. M. Thornley, Rep. Prog. Phys. **29**, 675 (1966); C. L. Ballhausen and H. B. Gray, *Molecular Orbital Theory* (Benjamin, New York, 1964).

[29]F. Herman and S. Skillman, *Atomic Structure Calculations* (Prentice-Hall, Englewood Cliffs, NJ, 1983).

[30]R. E. Watson, Phys. Rev. **111**, 1108 (1958).

[31]C. J. Toussaint, J. Appl. Crystallogr. **4**, 293 (1971).

[32]G. Srinavasan and M. S. Seehra, Phys. Rev. B **29**, 6295 (1984); W. L. Roth, Phys. Rev. **110**, 1333 (1958); **111**, 772 (1958); J. Appl. Phys. **31**, 2000 (1960); H. La Blanchetais, J. Phys. Radium **12**, 765 (1951); J. R. Singer, Phys. Rev. **104**, 929 (1956).

[33]L. F. Mattheis, Phys. Rev. B **2**, 3918 (1970).

[34]J. Hugel and C. Carabatos, J. Phys. C **16**, 6713 (1983).

[35]L. T. Wille, P. J. Durham, and P. A. Sterne, J. Phys. (Paris) Colloq. **47**, C8-43 (1986).

[36]D. G. Lock and R. N. West, Appl. Phys. **6**, 249 (1975).

[37]G. M. Beardsley, S. Berko, J. J. Mader, and M. A. Shulman, Appl. Phys. **5**, 375 (1975).

[38]R. N. West, J. Mayers, and P. A. Walters, J. Phys. E **14**, 478

(1981); A. A. Manuel, S. Samoilov, R. Sachot, P. Descouts, and M. Peter, Solid State Commun. **31**, 955 (1979); W. S. Farmer, F. Sinclair, S. Berko, and G. M. Beardsley, *ibid.* **31**, 481 (1979).

[39]J. H. Kaiser, P. A. Walters, C. R. Bull, A. Alam, R. N. West, and N. Shiotani, J. Phys. F **17**, 1243 (1988); J. H. Kaiser, R. N. West, and N. Shiotani, *ibid.* **16**, 1307 (1986).

[40]A. L. Wachs, P. E. A. Turchi, J. H. Kaiser, R. N. West, R. H. Howell, Y. C. Jean, Karl L. Merkle, Alexandre Revcolevschi, and M. J. Fluss, in Proceedings of the Eighth International Conference on Positron Annihilation, Gent, Belgium, 1988, (World Scientific, Singapore, in press).

[41]By analogy, positronic wave-function calculations for Si using the technique of Refs. 15, 18, and 19 show the positron mainly resides in the interstitial regions between the Si—Si covalent bonds [P. E. A. Turchi (unpublished) and R. N. West and J. H. Kaiser (unpublished)]; for discussions of positronic wave functions in La_2CuO_4 and $YBa_2Cu_3O_7$ see Refs. 13, 15, and 22.

[42]M. Peter, L. Hoffman, and A. A. Manuel, in Proceedings of the Eighth International Conference on Positron Annihilation, Gent, Belgium, 1988 (World Scientific, Singapore, in press); M. Peter (private communication).

[43]A. Bansil, R. Pankaluto, R. S. Rao, P. E. Mijnarends, W. Dlugosz, R. Prasad, and L. C. Smedskjaer, Phys. Rev. Lett. **61**, 2480 (1988).

[44]N. Shiotani (private communication).